Published in final edited form as:

Inorg Chem. 2016 June 20; 55(12): 6095–6099. doi:10.1021/acs.inorgchem.6b00630.

Effect of the Mn Oxidation State on Single-Molecule-Magnet Properties: Mn^{III} vs Mn^{IV} in Biologically Inspired $DyMn_3O_4$ Cubanes

Po-Heng Lin[†,‡], **Emily Y. Tsui**[†], **Fatemah Habib**[§], **Muralee Murugesu**[*,§], and **Theodor Agapie**[*,†]

[†]Division of Chemistry and Chemical Engineering, California Institute of Technology, Pasadena, California 91125, United States

[§]Department of Chemistry, University of Ottawa, 10 Marie-Curie, Ottawa, Ontario K1N 6N5, Canada

[‡]Department of Chemistry, National Chung Hsing University, 250 Kuo Kuang Road, Taichung 40227, Taiwan

Abstract

Inspired by the ferromagnetic coupling in the cubane model $CaMn^{IV}_3O_4$ of the oxygen-evolving complex of photosystem II, 3d–4f mixed-metal $DyMn_3O_4$ clusters were prepared for investigation of the magnetic properties. For comparison, $YMn^{IV}_3O_4$ and $YMn^{IV}_2Mn^{III}O_4$ clusters were investigated as well and showed ferromagnetic interactions, like the calcium analogue. $DyMn^{IV}_3O_4$ displays single-molecule-magnet properties, while the one-electron-reduced species ($DyMn^{IV}_2Mn^{III}O_4$) does not, despite the presence of a Mn^{III} center with higher spin and single-ion anisotropy.

Graphical abstract

[*]Corresponding Authors: m.murugesu@uottawa.ca. agapie@caltech.edu.

Notes

The authors declare no competing financial interest.

Supporting Information

The Supporting Information is available free of charge on the ACS Publications website at DOI: 10.1021/acs.inorgchem.6b00630.
Crystallographic data in CIF format (CIF)
Crystallographic data in CIF format (CIF)
Crystallographic data in CIF format (CIF)
Experimental procedures and spectroscopic characterization (PDF)

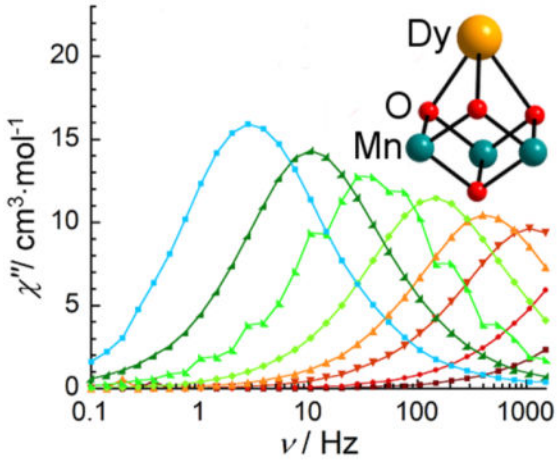

INTRODUCTION

Transition-metal lanthanide (3d–4f) clusters have shown promise as single-molecule-magnet (SMM) candidates.[1] The combination of high single-ion anisotropy of particular lanthanides and the high spin of multinuclear complexes provides a strategy for the synthesis of SMMs with large relaxation barriers.[2] Although the largest energy barriers of SMMs are found in mono- or dinuclear lanthanide complexes because of the weak exchange interactions of lanthanide ions,[3] coupling with transition metals has also been investigated to increase the relaxation barrier.[4] Despite the discovery of numerous 3d–4f SMMs, the rational design of molecules with improved SMM properties remains challenging, and the study toward a detailed understanding of the structural factors that control the SMM behavior is an active area of research.

We have reported the preparation of tetranuclear heterometallic MMn_3O_4 cubanes[5] as structural models of the oxygen-evolving complex of photosystem II that displays a $CaMn_4O_5$ cluster.[6] The $CaMn^{IV}{}_3O_4$ cubane, with a diamagnetic Ca^{2+}, displays predominantly ferromagnetic coupling between the transition-metal ions, with the higher-symmetry cubane showing smaller coupling constants.[7] The magnetic behavior of these clusters was studied computationally, and a high-spin ground state was concluded to be an intrinsic characteristic of the $CaMn^{IV}{}_3O_4$ heterometallic cubane motif because of its structural parameters, in particular the acute Mn–O–Mn angles.[8] The ferromagnetic coupling of the Mn_3 motif was envisioned to be a useful design element for the study of the magnetism of 3d–4f clusters.[9] A $CaMn^{IV}{}_3O_4$ precursor provides facile synthetic access by metal substitution to lanthanide-containing cubanes of interest related to SMMs.[5b] Access to two oxidation states, $LnMn^{IV}{}_3O_4$ and $LnMn^{IV}{}_2Mn^{III}O_4$, allows for evaluation of the impact of a single electron transfer on the SMM properties of the clusters. This is of particular interest given the potential for facile modulation of the magnetic properties via redox chemistry, but its effects on the 3d–4f SMM properties are poorly understood. Although manganese-only SMM studies of isostructural clusters with different Mn oxidation states have been performed,[10] similar investigations of 3d–4f mixed-metal complexes are rare. We

report herein on the magnetic properties of the Dy^{III} and Y^{III} versions of heterometallic cubanes.

RESULTS AND DISCUSSION

The heteronuclear complexes $[LY^{III}Mn^{IV}_3O_4(OAc)_3(DMF)_2]$-[OTf] (**1-Y**) and $[LDy^{III}Mn^{IV}_3O_4(OAc)_3(DMF)_2][OTf]$ (**1-Dy**), where DMF = *N,N*-dimethylformamide and $^{-}$OTf = trifluoromethanesulfonate, have been reported by us, including structural characterization for **1-Y**.[5b,c] The reduced species ($[LY^{III}Mn^{IV}_2Mn^{III}O_4(OAc)_3(DMF)]$ (**2-Y**) and $[LDy^{III}Mn^{IV}_2Mn^{III}O_4(OAc)_3(DMF)_2]$ (**2-Dy**)) were prepared by the treatment of a tetrahydrofuran (THF) suspension of a cationic precursor (**1-Y** and **1-Dy**, respectively) with 1 equiv of decamethylferrocene (Figure 1). Single-crystal X-ray diffraction studies were performed for compounds **1-Dy**, **2-Y**, and **2-Dy**. The top metal is eight-coordinate in compounds **1-Y**, **1-Dy**, and **2-Dy** with three acetates, three oxidos, and two DMF molecules completing the coordination sphere (Figure 2). **2-Y** displays a single DMF ligand, resulting in a seven-coordinate Y center (Figure 3). The Mn–O(oxido) distances are short and similar (1.84–1.91 Å) in **1-Y** and **1-Dy**, consistent with the all-Mn^{IV} assignment. Compounds **2-Y** and **2-Dy** (Figures 2 and 3) show elongation of the O5–Mn1 and O4–Mn1 distances (to >2.10 Å), consistent with a localized Mn^{III} site with population of a σ-antibonding orbital along this axis.

Direct-current (dc) magnetic susceptibility measurements were performed on **1-Y**, **2-Y**, **1-Dy**, and **2-Dy** between 1.8 and 300 K under an external field of 1000 Oe (Figure 4). The observed paramagnetic behavior of all four complexes arises from the 3d Mn^{III} and Mn^{IV} ions and/or 4f Ln^{III} ions. The experimentally obtained χT values are 5.67, 9.02, 20.78, and 25.02 $cm^3{\cdot}K{\cdot}mol^{-1}$ for complexes **1-Y**, **2-Y**, **1-Dy**, and **2-Dy**, respectively. According to the free-ion approximation of each metal ion [Dy^{III} ($^6H_{15/2}$, $S = {}^5/_2$, $L = 5$, $g = {}^4/_3$, χT = 14.17 $cm^3{\cdot}K{\cdot}mol^{-1}$), Mn^{III} ($S = 2$; $g = 2.00$, χT = 3.00 $cm^3{\cdot}K{\cdot}mol^{-1}$), and Mn^{IV} ($S = {}^3/_2$; $g = 2.00$, χT = 1.875 $cm^3{\cdot}K{\cdot}mol^{-1}$)], the theoretical values for four noninteracting metal ions are calculated to be 5.63, 6.75, 19.80, and 20.92 $cm^3{\cdot}K{\cdot}mol^{-1}$ for complexes **1-Y**, **2-Y**, **1-Dy**, and **2-Dy**, respectively. The different χT values between the experimental and theoretical values for **2-Y** and **2-Dy** may be due to residual solvents in the samples that were also observed by combustion analysis. The χT values observed for **2-Y** and **2-Dy** are higher than those for **1-Y** and **1-Dy**, respectively, confirming that one Mn^{IV} ion in the cubane was reduced. Upon a decrease in the temperature, the χT products remain fairly constant down to ~70 K for all complexes. The χT values then increase to a maximum value for **1-Dy** and **1-Y** around 6 K because of intramolecular ferromagnetic interactions and then slightly decrease at lower temperature likely because of intermolecular antiferromagnetic interactions. The χT values of **2-Dy** decreasing gradually below 70 K are presumably due to the presence of large magnetoanisotropy in the Dy^{III} system, which was not observed in **2-Y**. Both χT values of **2-Dy** and **2-Y** increase at lower temperatures to maximum values of 23.70 $cm^3{\cdot}K{\cdot}mol^{-1}$ (at 6 K) and 10.57 $cm^3{\cdot}K{\cdot}mol^{-1}$ (at 5.5 K) for **2-Dy** and **2-Y**, respectively, which are indicative of ferromagnetic interactions between the metal ions within the $LnMn_3$ unit. A slight decrease at lower temperatures (with values of 21.30 and

10.02 $cm^3 \cdot K \cdot mol^{-1}$ at 2 K for **2-Dy** and **2-Y**, respectively) indicates intermolecular antiferromagnetic interactions.

The amplitude of the increase of the χT values suggests weak coupling between metal ions in the reduced compounds. Considering the number of magnetic exchange pathways between metal centers as well as the presence of the highly anisotropic Dy^{III} ion renders modeling of **1-Dy** and **2-Dy** difficult. Therefore, complexes **1-Y** and **2-Y** containing the diamagnetic Y^{III} ion become ideal models for probing the overall exchange interactions between the Mn ions.

The magnetic susceptibility data can be fit to obtain the nature and magnitude of the magnetic interaction between Mn^{III} and/or Mn^{IV}. By using the isotropic spin Hamiltonian $\hat{H} = -2J(\hat{S}_1 \cdot \hat{S}_2 + \hat{S}_1 \cdot \hat{S}_3) - 2J'(\hat{S}_2 \cdot \hat{S}_3)$ with $S_1 = S_2 = S_3 = {}^3/_2$ for **1-Y** and $S_1 = 2$, $S_2 = S_3 = {}^3/_2$ for **2-Y** (Scheme S1), the best-fit parameters obtained are $J = 5.35\ cm^{-1}$, $J' = -0.81\ cm^{-1}$, $g = 1.93$, and $S = {}^9/_2$ (**1-Y**) and $J = 0.78\ cm^{-1}$, $J' = -0.98\ cm^{-1}$, $g = 2.31$, and $S = 5$ (**2-Y**) (Figure S1 and Scheme S1), showing ferromagnetic contributions, similar to experimental and computed $CaMn_3O_4$ cubane systems, albeit with small coupling constants.[7,8] Although the fit parameters did not include the anisotropy of the Mn^{III} ions and despite the fitting being slightly different from that of the experimental data, it is estimated that the ferromagnetic interaction between Mn^{IV} ions in **1-Y** is slightly larger than the interaction between Mn^{III} and Mn^{IV} in **2-Y**, which agrees well with the values reported for other Mn^{III}/Mn^{IV} isostructural systems.[11] We can further assess the interactions between Dy^{III} and Mn^{III} or Mn^{IV} by subtracting χT values of **1-Y** and **2-Y** from **1-Dy** and **2-Dy** to give suitably adjusted plots (green circles, Figure 4 and inset).

The field dependences (up to 7 T) of the magnetization of all four complexes in the temperature range of 1.8–7 K were also obtained (Figure 5). The saturation of the magnetization suggests the absence of significant magnetic anisotropy, consistent with three Mn^{IV} ions in compound **1-Y**. The magnetization at 1.8 K saturates above 5.5 T at 8.5 μ_B, which is lower than those of the other trinuclear Mn^{IV} complexes. The Dy–Mn interactions of **1-Dy** are much stronger than those of **2-Dy** based on the larger maximum χT value and the sharper increase at low temperature. This magnetic effect corresponds to shorter Dy–O(oxido) distances in **2-Dy** [2.294(2), 2.385(2), and 2.389(2) Å] compared to those in **1-Dy** [2.355(1), 2.400(1), and 2.443(1) Å]. The reasons behind this structural change and its influence on magnetism are not understood but could include an increase in the electron density on the Mn centers due to reduction, leading to weaker Mn–O interactions and stronger Dy–O interactions; however, this proposal is not substantiated by a lengthening of the Mn–O(oxido Dy) distances in **2-Dy**.

In order to probe the possible SMM behavior in **1-Dy**, **2-Dy**, and **2-Y**, the temperature dependences of the in-phase (χ') and out-of-phase (χ'') magnetic susceptibilities were measured in the temperature range of 2–5 K. Only **1-Dy** exhibited a temperature-and frequency-dependent signal indicating slow relaxation of the magnetization under a zero dc field and a 3 Oe oscillating field at frequencies between 1 and 1500 Hz as expected for an SMM (Figure 6). For **1-Dy**, the maxima can be observed for a range of temperatures between 3 and 1.8 K. The relaxation time deduced from this data is consistent with an

activated behavior (Figure 6, inset), with an anisotropic energy barrier (U_{eff}) of 27 K and a preexponential factor (τ_0) of 2.13×10^{-8} s. The peaks of **1-Dy** in χ'') versus ν are shifted under the various dc fields, but the alternating-current (ac) measurements under the applied optimum field of 800 Oe only reveal a slightly higher energy barrier (Figures S2–S4). In contrast to **1-Dy**, there is no evidence that the one-electron-reduced species **2-Dy** is an SMM (Figures S5 and S6). The observed frequency-independent χ'' signal with a large applied dc field is likely due to an intermolecularly driven relaxation process.[12] We also measured the ac susceptibility for **2-Y** because of the anisotropic nature of the Mn^{III} ion, but no out-of-phase signals were observed, indicating that the Mn centers alone are not sufficient for SMM properties in this geometry.

On the basis of a comparison of the dc and ac data of **1-Dy** and **2-Dy**, the interaction between the Dy and Mn ions is key to the SMM properties in these compounds. Even though a Mn^{III} ion has magnetoanisotropy due to Jahn–Teller distortion and one more unpaired electron than Mn^{IV}, the SMM properties of our 3d–4f cubane system were not improved when one Mn^{IV} was reduced to Mn^{III}. A significantly higher χT value for **1-Dy** compared to that of **2-Dy** at 6 K indicates a stronger 3d–4f ferromagnetic interaction, with a larger spin ground state being likely. Because of the presence of significant spin–orbit coupling of the Dy^{III} ion, no fits have been made to date. It is reasonable to assume that, in addition to a larger spin ground state, significantly stronger coupling will likely provide a well-defined ground state with the first excited state higher in energy, leading to enhanced SMM behavior for **1-Dy**.

Additionally, the different Dy–ligand interactions and change in the coordination environment induced by the reduction could affect the Dy-ion anisotropy. To validate this, Magellan magnetic software[11] was employed to probe the anisotropy axis direction on the Dy^{III} ions. The modeled anisotropy axes of Dy^{III} (Figure 7) give an indication that, in the case of **2-Dy**, the anisotropy on the Dy center is nearly perpendicular to the anisotropy of the Mn^{III} ion (the Jahn–Teller elongation axis highlighted in black); this reduces the overall anisotropy of the system. In this case, the addition of anisotropic Mn^{III} ions can have an effect on the weaker interactions between Dy^{III} and Mn^{IV}/Mn^{III}, which may decrease the spin ground state (S_T) as well as lower the overall anisotropy of the complex, which reduced the Ising-type magnetoanisotropy (D) and thus decreased the SMM performance.

CONCLUSION

In summary, the heterometallic 3d–4f Mn/Dy and Mn/Y clusters $LnMn^{IV}{}_3O_4$ were reduced by one electron to form $LnMn^{IV}{}_2Mn^{III}O_4$ species that maintain the cubane motif and show a localized Mn^{III} site with corresponding metal–ligand distortions. The $YMn^{IV}{}_3O_4$ cubane (**1-Y**) displays ferromagnetism, supporting the notion that this is a characteristic property of $MMn^{IV}{}_3O_4$ cubanes, as was previously computed for the biologically relevant $CaMn^{IV}{}_3O_4$ cluster. The related $DyMn^{IV}{}_3O_4$ (**1-Dy**) and $DyMn^{IV}{}_2Mn^{III}O_4$ (**2-Dy**) clusters offer suitable models for studying the effect of the oxidation state of Mn in the SMM behavior of 3d–4f clusters. **2-Dy** is not an SMM despite the presence of an additional electron and of a Mn^{III} center with magnetoanisotropy. The ferromagnetic interactions within the $Mn_3{}^{IV}$ core and

the nonnegligible Dy–Mn interactions result in a large spin ground state, contributing to the SMM properties of **1-Dy**.

EXPERIMENTAL SECTION

Reactions performed under an inert atmosphere were carried out in oven-dried glassware in a glovebox under a nitrogen atmosphere. Anhydrous dichloromethane and diethyl ether were purified by sparging with nitrogen for 15 min and then passing under nitrogen pressure through a column of activated A2 alumina (Zapp's). CD_2Cl_2 was purchased from Cambridge Isotope Laboratories, dried over calcium hydride, then degassed by three freeze–pump–thaw cycles, and vacuum-transferred prior to use. ^{1}H NMR spectra were recorded on a Varian 300 MHz instrument, with shifts reported relative to the residual solvent peak. ^{19}F NMR spectra were recorded on a Varian 300 MHz instrument, with shifts reported relative to the internal lock signal. Elemental analyses were performed by Robertson Microlit Laboratories. All commercial chemicals were used as received. Dysprosium trifluoromethanesulfonate ($Dy(OTf)_3$) and decamethylferrocene were purchased from Strem, and yttrium trifluoromethanesulfonate (Y-$(OTf)_3$) was purchased from Aldrich. $[LDyMn_3O_4(OAc)_3(DMF)_2]$-[OTf][5b] and $[LYMn_3O_4(OAc)_3(DMF)_2][OTf]$[5c] were prepared according to previously published procedures.

Synthesis of $[LDyMn_3O_4(OAc)_3(DMF)_2]$ (2-Dy)

A solution of decamethylferrocene (0.007 g, 0.02 mmol, 1 equiv) in THF (2 mL) was added to a solution of **1-Dy** (0.034 g, 0.02 mmol, 1 equiv) in THF (2 mL). The dark-brown solution was stirred overnight. The dark-brown precipitate generated was collected on a fritted glass funnel, washed with acetonitrile (4 mL) to remove the remaining decamethylferrocenium triflate, and further washed with dichloromethane. The resulting brown powder was dissolved in benzene/THF and concentrated in vacuo. Recrystallization from DMF/benzene/ether yields the product as dark-brown crystals (0.009 g, 29%). ^{1}H NMR (C_6D_6, 300 MHz): δ 7.2, 3.4, 1.6, 1.2, −2.4. Anal. Calcd for $C_{73}H_{63}Cl_2DyMn_3N_7O_{14}$([**2-Dy**]·$CH_2Cl_2$·$C_6H_6$): C, 52.65; H, 4.07; N, 6.46. Found: C, 52.49; H, 3.72; N, 5.96.

Synthesis of $[LYMn_3O_4(OAc)_3(DMF)]$ (2-Y)

A solution of decamethylferrocene (0.017 g, 0.0527 mmol) in THF (2 mL) was added to a solution of **1-Y** (0.079 g, 0.0527 mmol, 1 equiv) in THF (8 mL). The mixture was stirred at room temperature for 30 min and then filtered through Celite. The filtrate was dried in vacuo. Benzene was added, and the mixture was filtered through Celite to remove decamethylferrocenium triflate. The benzene filtrate was dried in vacuo to yield the product as a red-brown solid (0.063 g, 94%). X-ray-quality crystals were grown by vapor diffusion of diethyl ether into a DMF solution of **2-Y**. ^{1}H NMR (C_6D_6, 300 MHz): δ 25.1, 13.1, 11.3, 10.2, 9.3, 7.8, 5.5, 4.5, −25.3. Anal. Calcd for $C_{66}H_{55}Mn_3N_7O_{14}Y$: C, 55.67; H, 3.89; N, 6.89. Anal. Calcd for $C_{69}H_{62}Mn_3N_8O_{15}Y$ (one DMF solvate): C, 55.36; H, 4.17; N, 7.49. Found: C, 53.96; H, 4.88; N, 7.26.

Magnetic Measurements

The magnetic susceptibility measurements were obtained using a Quantum Design SQUID MPMS-XL7 magnetometer operating between 1.8 and 300 K for dc applied fields ranging from −7 to +7 T. dc analyses were performed on polycrystalline samples of 7.3, 13.0, 18.0, and 25.0 mg for **1-Dy**, **2-Dy**, **1-Y**, and **2-Y**, respectively, restrained in a polyethylene membrane and under a field ranging from 0 to 7 T between 1.8 and 300 K. ac susceptibility measurements were carried out under an oscillating ac field of 3 Oe and ac frequencies ranging from 1 to 1500 Hz. The magnetization data were collected at 100 K to check for ferromagnetic impurities that were absent in all samples. A diamagnetic correction was applied for the sample holder and the sample.

Supplementary Material

Refer to Web version on PubMed Central for supplementary material.

Acknowledgments

We thank Caltech, the NIH (Grant R01 GM102687A), and a Sandia Campus Executive Fellowship (to E.Y.T.) for financial support. T.A. is grateful for Sloan, Cottrell, and Dreyfus scholarships. We also thank R. Holmberg for Magellan analysis.

References

1. (a) Sharples JW, Collison D. Coord Chem Rev. 2014; 260:1–20. [PubMed: 25009361] (b) Winpenny REP. Chem Soc Rev. 1998; 27:447–452.(c) Rosado Piquer L, Sanudo EC. Dalton Trans. 2015; 44:8771–8780. [PubMed: 25847327] (d) Liu K, Shi W, Cheng P. Coord Chem Rev. 2015; 289–290:74–122.(e) Andruh M, Costes JP, Diaz C, Gao S. Inorg Chem. 2009; 48:3342–3359. [PubMed: 19361237]
2. (a) Funes AV, Carrella L, Rentschler E, Albores P. Dalton Trans. 2014; 43:2361–2364. [PubMed: 24343381] (b) Langley SK, Ungur L, Chilton NF, Moubaraki B, Chibotaru LF, Murray KS. Inorg Chem. 2014; 53:4303–4315. [PubMed: 24749511] (c) Li XL, Min FY, Wang C, Lin SY, Liu Z, Tang J. Dalton Trans. 2015; 44:3430–3438. [PubMed: 25601415]
3. (a) Fatila EM, Clerac R, Rouzieres M, Soldatov DV, Jennings M, Preuss KE. J Am Chem Soc. 2013; 135:13298–13301. [PubMed: 23984987] (b) Le Roy JJ, Jeletic M, Gorelsky SI, Korobkov I, Ungur L, Chibotaru LF, Murugesu M. J Am Chem Soc. 2013; 135:3502–3510. [PubMed: 23391235] (c) Pointillart F, Le Guennic B, Golhen S, Cador O, Ouahab L. Chem Commun. 2013; 49:11632–11634.(d) Rinehart JD, Fang M, Evans WJ, Long JR. Nat Chem. 2011; 3:538–542. [PubMed: 21697874]
4. (a) Liu JL, Chen YC, Zheng YZ, Lin WQ, Ungur L, Wernsdorfer W, Chibotaru LF, Tong ML. Chem Sci. 2013; 4:3310–3316.(b) Sun W-B, Yan P-F, Jiang S-D, Wang B-W, Zhang Y-Q, Li H-F, Chen P, Wang Z-M, Gao S. Chem Sci. 2016; 7:684–691.
5. (a) Kanady JS, Tsui EY, Day MW, Agapie T. Science. 2011; 333:733–736. [PubMed: 21817047] (b) Lin PH, Takase MK, Agapie T. Inorg Chem. 2015; 54:59–64. [PubMed: 25521310] (c) Tsui EY, Agapie T. Proc Natl Acad Sci U S A. 2013; 110:10084–10088. [PubMed: 23744039]
6. Suga M, Akita F, Hirata K, Ueno G, Murakami H, Nakajima Y, Shimizu T, Yamashita K, Yamamoto M, Ago H, Shen JR. Nature. 2014; 517:99–103. [PubMed: 25470056]
7. (a) Kanady JS, Mendoza-Cortes JL, Tsui EY, Nielsen RJ, Goddard WA, Agapie T. J Am Chem Soc. 2013; 135:1073–1082. [PubMed: 23241061] (b) Mukherjee S, Stull JA, Yano J, Stamatatos TC, Pringouri K, Stich TA, Abboud KA, Britt RD, Yachandra VK, Christou G. Proc Natl Acad Sci U S A. 2012; 109:2257–2262. [PubMed: 22308383]
8. Krewald V, Neese F, Pantazis D. A J Am Chem Soc. 2013; 135:5726–5739. [PubMed: 23527603]

9. Lampropoulos C, Stamatatos TC, Abboud KA, Christou G. Inorg Chem. 2009; 48:429–431. [PubMed: 19072591]

10. (a) Habib F, Brunet G, Loiseau F, Pathmalingam T, Burchell TJ, Beauchemin AM, Wernsdorfer W, Clerac R, Murugesu M. Inorg Chem. 2013; 52:1296–303. [PubMed: 23343331] (b) Soler M, Wernsdorfer W, Abboud KA, Huffman JC, Davidson ER, Hendrickson DN, Christou G. J Am Chem Soc. 2003; 125:3576–3588. [PubMed: 12643720] (c) Jones LF, Inglis R, Cochrane ME, Mason K, Collins A, Parsons S, Perlepes SP, Brechin EK. Dalton Trans. 2008:6205–6210. [PubMed: 18985253]

11. Pathmalingam T, Gorelsky SI, Burchell TJ, Bedard AC, Beauchemin AM, Clerac R, Murugesu M. Chem Commun. 2008:2782–2784.

12. Habib F, Korobkov I, Murugesu M. Dalton Trans. 2015; 44:6368–6373. [PubMed: 25742046]

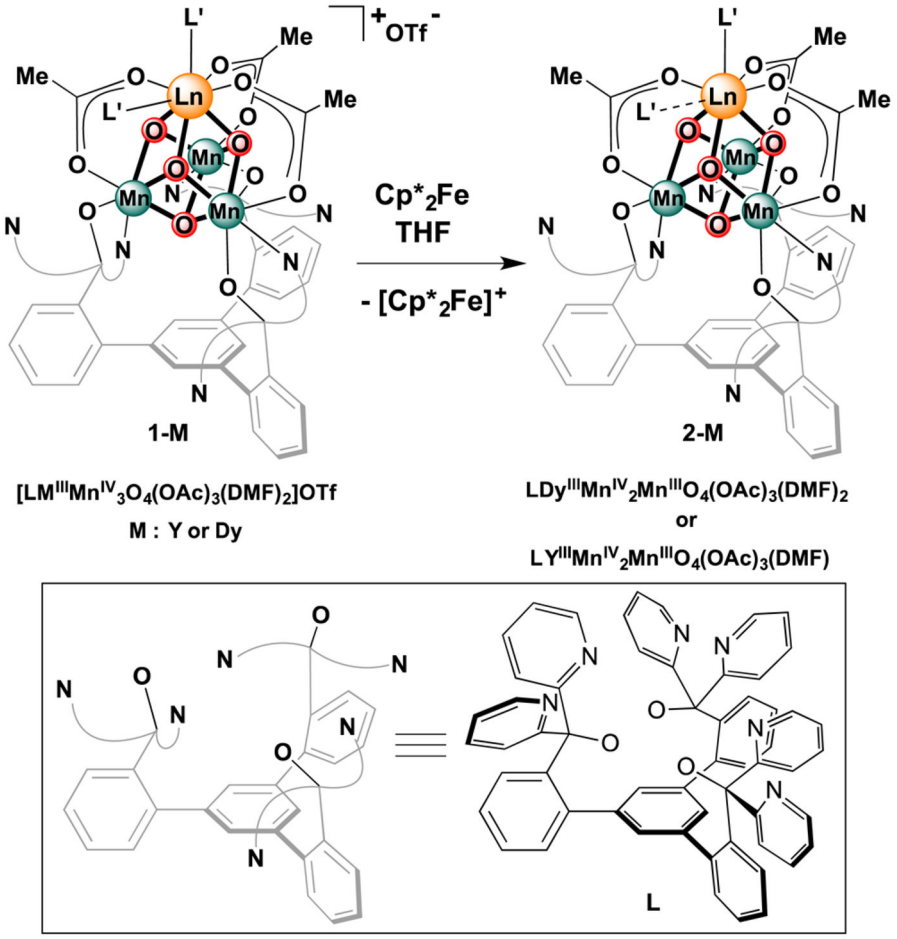

Figure 1.
Synthesis of reduced cubane complexes.

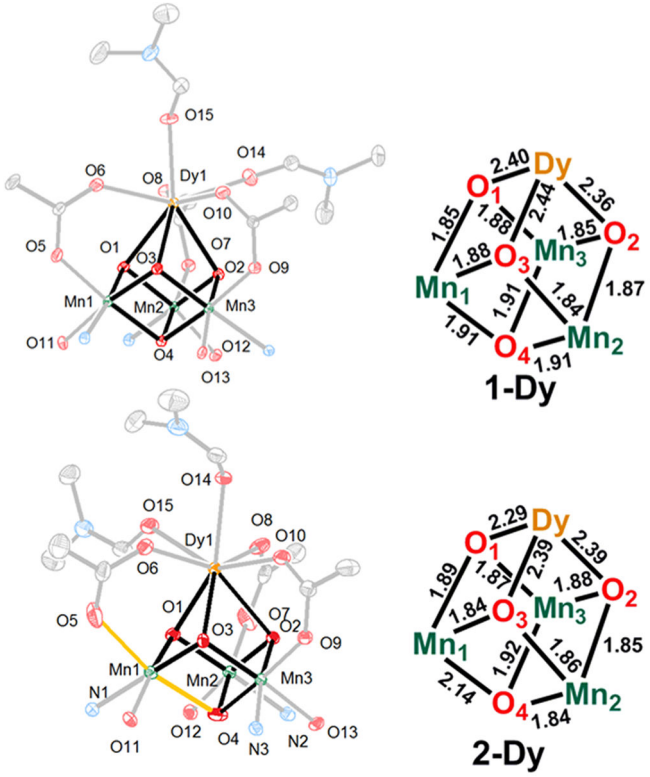

Figure 2.

Left: Cluster thermal ellipsoid plot for 1-Dy (top) and 2-Dy (bottom). H atoms, solvent molecules, counteranions, and parts of the ligand are not shown for clarity. The elongated Mn–O bonds in 2-Dy are highlighted in orange. Right: Bond distances (Å) in the cubane core.

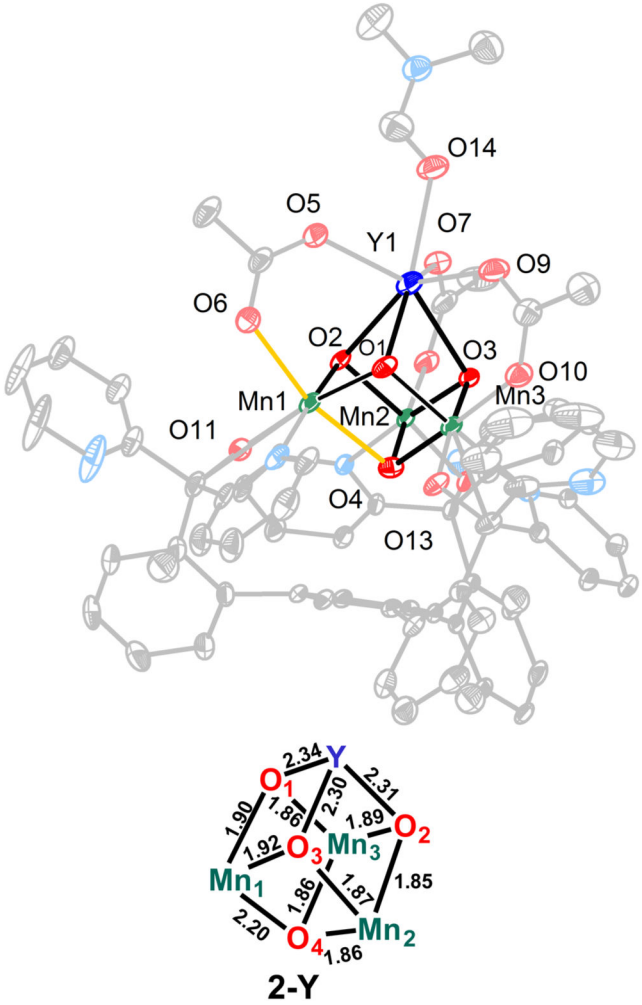

Figure 3.

Top: Thermal ellipsoid plot for 2-Y. H atoms, solvent molecules, and counteranions are not shown for clarity. The elongated Mn–O bonds in 2-Y are highlighted in orange. Bottom: Bond distances (Å) in the cubane core.

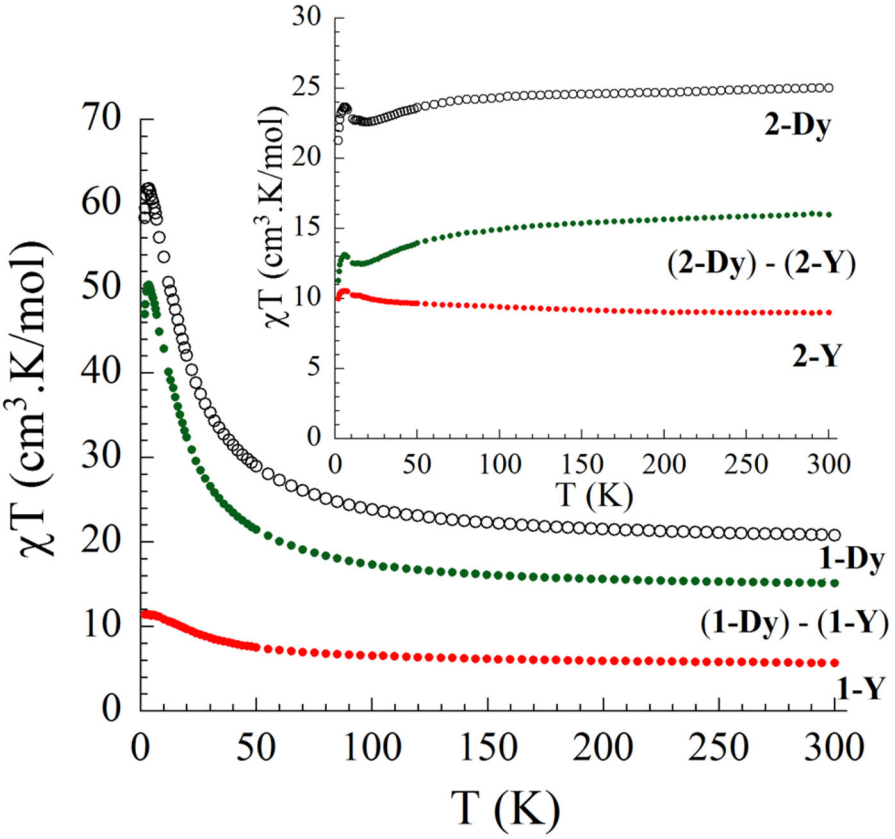

Figure 4.

Temperature dependence of the χT product at 1000 Oe for 1-Dy (black), 2-Dy (black inset), 1-Y (red), and 2-Y (red inset). The green dots represent the values of 1-Y and 2-Y subtracted from 1-Dy and 2-Dy, respectively. χ is the molar susceptibility per cubane complex defined as *M/H*.

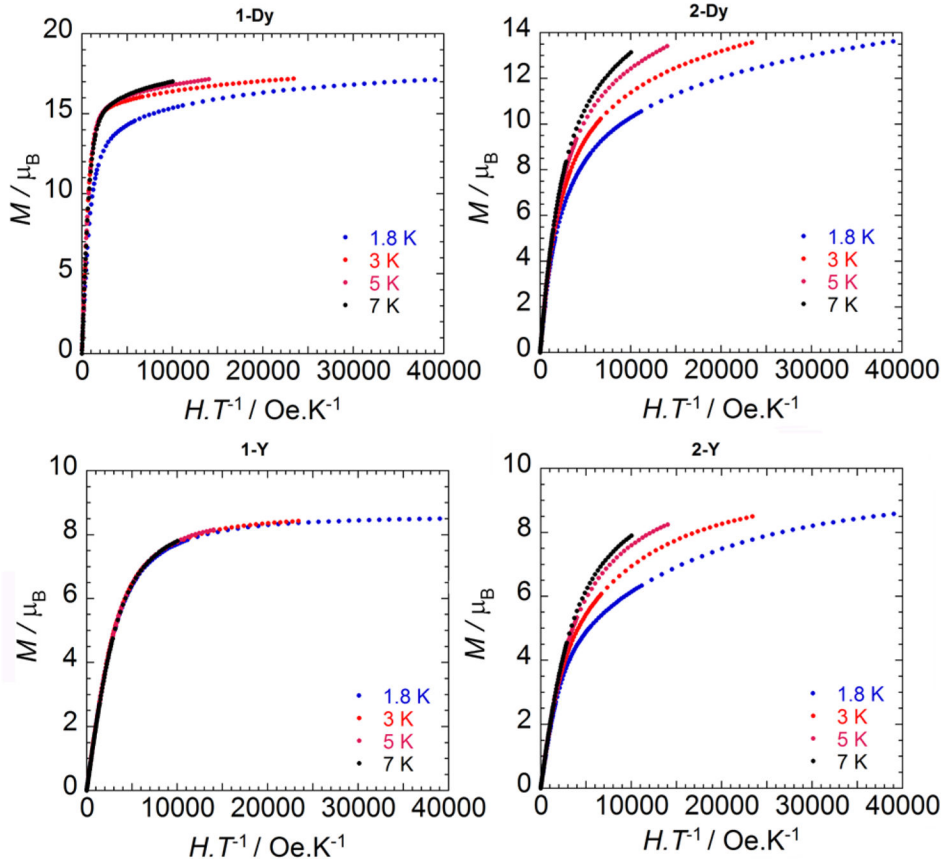

Figure 5.
Field dependences of the magnetization at variable temperatures for the reported complexes.

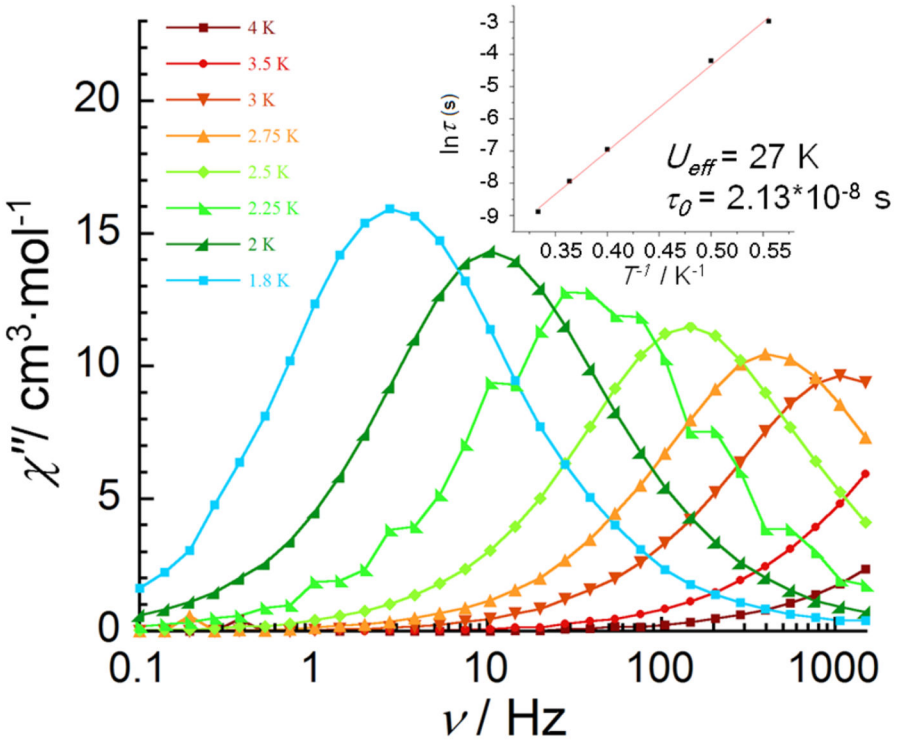

Figure 6.

Temperature dependence of the out-of-phase (χ'') ac susceptibility of 1-Dy from 0.1 to 1500 Hz without an applied dc field. Inset: Arrhenius plot, ln(τ) versus 1/T. The red line indicates the fit yielding the energy barrier for spin reversal.

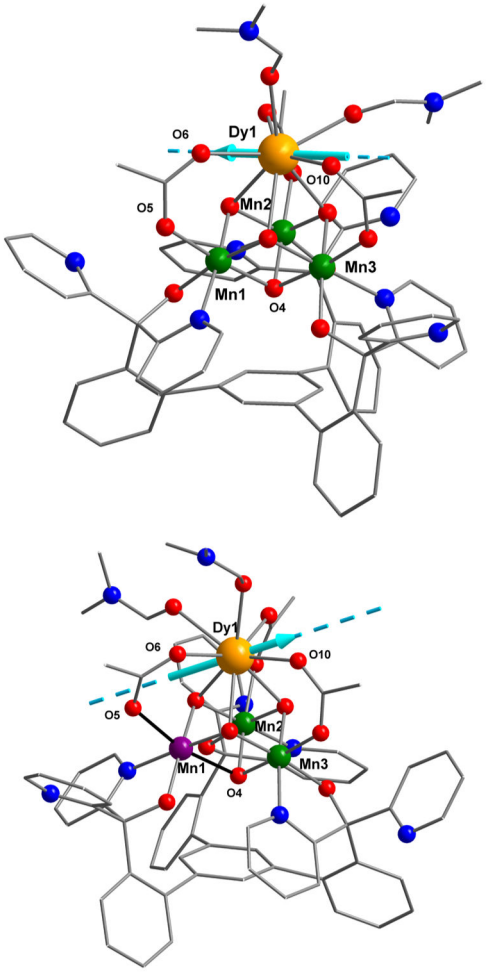

Figure 7.

Pictures of 1-Dy (top) and 2-Dy (bottom) containing the anisotropy axis direction for the Dy ions. The axes were modeled using Magellan magnetic software.[11]